HHS Public Access

Author manuscript

Free Radic Biol Med. Author manuscript; available in PMC 2017 June 01.

Published in final edited form as:

Free Radic Biol Med. 2016 June ; 95: 43–54. doi:10.1016/j.freeradbiomed.2016.02.032.

Glutathione-Deficient *Plasmodium berghei* Parasites Exhibit Growth Delay and Nuclear DNA Damage

Vivian Padín-Irizarry[1,2], **Emilee E. Colón-Lorenzo**[1], **Joel Vega-Rodríguez**[1,3], **María del R. Castro**[4], **Ricardo González-Méndez**[5], **Sylvette Ayala-Peña**[4,#], and **Adelfa E. Serrano**[1,#,*]

[1]Department of Microbiology and Medical Zoology, University of Puerto Rico, School of Medicine, San Juan 00936-5067, PR

[4]Department of Pharmacology and Toxicology, University of Puerto Rico, School of Medicine, San Juan 00936-5067, PR

[5]Department of Radiological Sciences, University of Puerto Rico, School of Medicine, San Juan 00936-5067, PR

Abstract

Plasmodium parasites are exposed to endogenous and exogenous oxidative stress during their complex life cycle. To minimize oxidative damage, the parasites use glutathione (GSH) and thioredoxin (Trx) as primary antioxidants. We previously showed that disruption of the *Plasmodium berghei* gamma-glutamylcysteine synthetase (*pbggcs-ko*) or the glutathione reductase (*pbgr-ko*) genes resulted in a significant reduction of GSH in intraerythrocytic stages, and a defect in growth in the *pbggcs-ko* parasites. In this report, time course experiments of parasite intraerythrocytic development and morphological studies showed a growth delay during the ring to schizont progression. Morphological analysis shows a significant reduction in size (diameter) of trophozoites and schizonts with increased number of cytoplasmic vacuoles in the *pbggcs-ko* parasites in comparison to the wild type (WT). Furthermore, the *pbggcs-ko* mutants exhibited an impaired response to oxidative stress and increased levels of nuclear DNA (nDNA) damage. Reduced GSH levels did not result in mitochondrial DNA (mtDNA) damage or protein carbonylations in neither *pbggcs-ko* nor *pbgr-ko* parasites. In addition, the *pbggcs-ko* mutant

*Corresponding author, adelfa.serrano@upr.edu.
[2]Present address: Department of Global Health, University of South Florida, Tampa, Florida 33612, USA
[3]Present address: The W. Harry Feinstone Department of Molecular Microbiology and Immunology, Malaria Research Institute, Bloomberg School of Public Health, Johns Hopkins University, Baltimore, Maryland 21205, USA.
[#]Both authors contributed equally to this work

Competing interests

The authors have no competing interests to declare.

Authors' contribution

Conceived and designed the experiments: JVR EECL RGM SAP AES
Performed the experiments: VPI EECL MRC
Analyzed the data: VPI EECL RGM SAP AES
Contributed reagents/materials/analysis tools: AES
Wrote the paper: VPI EECL SAP AES
Revised the article critically: JVR RGM

parasites showed an increase in mRNA expression of genes involved in oxidative stress detoxification and DNA synthesis, suggesting a potential compensatory mechanism to allow for parasite proliferation. These results reveal that low GSH levels affect parasite development through the impairment of oxidative stress reduction systems and damage to the nDNA. Our studies provide new insights into the role of the GSH antioxidant system in the intraerythrocytic development of *Plasmodium* parasites, with potential translation into novel pharmacological interventions.

Keywords

Plasmodium berghei; malaria; glutathione; oxidative stress; growth delay; DNA damage; protein carbonylations

Introduction

Malaria remains the most deadly parasitic disease resulting in approximately 584,000 deaths from 198 million clinical cases reported in 2013 and one third of the world population at risk of infection [1]. This disease is caused by the apicomplexan parasites of the genus *Plasmodium*, which are transmitted to humans by the bite of infected *Anopheles* mosquitoes.

Plasmodium parasites are exposed to multiple sources of oxidative stress throughout their complex life cycle. During the intraerythrocytic development, endogenous oxidative stress results from reactive oxygen species (ROS) produced during hemoglobin (Hb) digestion in the parasite's food vacuole [2, 3]. In addition, the parasite is exposed to exogenous oxidative stress when merozoites egress from the red blood cells (RBC), inducing the production of nitric oxide and ROS by the host's immune system [2, 4]. *Plasmodium* parasites depend on two major NADPH-dependent redox networks, the GSH and the Trx antioxidant systems, to detoxify ROS and prevent oxidative damage [5].

Plasmodium synthesizes GSH by the sequential action of the rate limiting enzyme γ-glutamylcysteine synthetase (γ-GCS), and the glutathione synthetase [6]. The reduced GSH is oxidized to GSH disulfide (GSSG) by the reduction of glutaredoxin or glutathione-S-transferase (GST) [3, 6, 7]. The oxidized GSSG is reduced back to GSH by the glutathione reductase (GR), maintaining the GSH/GSSG ratio in the cell [8]. Glutathione plays an important role in a wide range of cellular processes including the detoxification of xenobiotics and protection against ROS [7, 9, 10]. In *Plasmodium* parasites, GSH is also involved in the degradation of the toxic ferritoprotoporphyrin IX (FP IX), escaped from hemozoin formation [11]. Additionally, GSH functions as an electron donor for the enzyme ribonucleotide reductase (RNR), [12, 13], crucial for DNA synthesis and cellular proliferation [2, 3, 10].

Previous reports from our laboratory demonstrated that disruption of the *pbggcs* gene in *Plasmodium berghei* resulted in mutant parasites displaying reduced GSH levels and growth impairment during intraerythrocytic development [14]. Moreover, disruption of the *pbggcs* gene inhibited oocyst development and the production of sporozoites in the mosquito, indicating that GSH biosynthesis is critical to complete parasite transmission [14]. Similarly,

P. berghei parasites with a disrupted glutathione reductase (*pbgr-ko*) gene displayed significantly reduced GSH levels and interruption of parasite development in the mosquito, with parasites arrested at the oocyst stage [15]. Although the relevance of GSH for parasite development has been shown, the underlying mechanisms of the delayed parasite development as a consequence of reduced GSH levels as well as the oxidative status of the mutant parasites deserves further investigation.

In this study, we further characterized the effects of reduced GSH levels in *P. berghei* and demonstrate that parasites with significantly low levels of GSH show a growth delay during the ring to schizont transition, have significantly smaller trophozoites and schizonts and a vacuolated cytoplasm. These changes occur concomitantly with an impairment capacity to handle oxidative stress and increased levels of nDNA damage. These results show for the first time a causal interplay between low GSH levels, impaired response to oxidative stress, oxidative DNA damage, and delayed parasite growth during the ring to schizont transition. The findings presented herein provide a better understanding of the need for maintaining GSH homeostasis during *P. berghei* development. Because the redox balance plays a vital role for parasite survival, our results have important applications for antimalarial treatments. Strategies aiming to promote oxidative stress and/or inhibiting the parasite antioxidant system will lead to a redox imbalance affecting parasite growth, and therefore a potential improvement in treatment response.

Materials and Methods

Mice and *P. berghei* lines

Random-bred Swiss albino CD-1 female mice (Charles River Laboratories, Wilmington, MA, USA), 6–8 weeks old, weighing 20–35 g were used for the study. All mice procedures were conducted at the AAALAC accredited University of Puerto Rico Medical Sciences Campus (UPR-MSC) Animal Resources Center and approved by the Institutional Animal Care and Use Committee (IACUC). All work was done in strict accordance with the “Guide for the Care and Use of Laboratory Animals” (National-Research-Council, Current Edition) and regulations of the PHS Policy on Humane Care and Use of Laboratory Animals. Mice were maintained and housed according to NIH and AAALAC regulations and guidelines. Mice were allowed to acclimatize for 1 week prior to the beginning of the studies. The *P. berghei* ANKA WT, reference line (507cl1), which expresses green fluorescent protein under the control of the constitutive *eukaryotic elongation factor 1A* promoter, was used as a control in all experiments [16]. The following *P. berghei* lines (mutants) were included in the study: *pbggcs-ko1* and *pbggcs-ko2* [14], and *pbgr-ko1* and *pbgr-ko2* [15].

Intraerythrocytic growth assay

To investigate the delayed parasitemia of *pbggcs-ko* parasites in mice [14], WT and *pbggcs-ko* parasites were synchronized in *in vitro* cultures as described by Janse and Waters [17]. Briefly, *P. berghei* infected blood was harvested from mice with 5–15% parasitemia, diluted in complete medium [RPMI 1640 (Gibco), 25% heat inactivated fetal bovine serum (Gibco), 50 IU/ml of neomycin (Sigma)] and cultured for 24–26 h at 37°C in an atmosphere of 10% O_2, 5% CO_2 and 85% N_2 gas mixture. The schizonts were purified by 55%

Nycodenz gradient [17] and injected intravenously into mice [18]. The synchronized ring infected blood was collected from mice 4–6 h post infection and cultured *in vitro* for a total of 28 h. The parasite intraerythrocytic development was analyzed by light microscopy of Diff-Quick stained thin smears in samples collected every 2 h, beginning after the initial 16 h of culture. Parasite intraerythrocytic developmental stages (rings, trophozoites and schizonts) and morphology were determined by counting at least 100 parasites per slide. Images were acquired with a microscope (BX51, Olympus) at 100X magnification using a digital camera (DP72, Olympus). The size of trophozoites and schizonts stages was assessed at 16, 24 and 28 h and vacuoles at 16 h in WT, *pbggcs-ko1* and *pbggcs-ko2* parasites using a calibrated ocular micrometer at 100X magnification (n=20).

Determination of intraparasitic response to oxidative stress levels by measuring the oxidation of 2′, 7′-dichlorodihydrofluorescein (DCFH)

To determine the levels of intraparasitic response to oxidative stress, the fluorescent intensity of dichlorofluorescein (DCF), the green fluorescent oxidation product of DFCH, was determined in WT and *pbggcs-ko* parasites cultured *in vitro*. The DCF fluorescent intensity was measured in the basal (untreated) or hydrogen peroxide (H_2O_2)-treated cultures as described by Trivedi *et al.* [19]. Briefly, *P. berghei* infected blood was cultured, as previously described, in the presence or absence of 2 mM H_2O_2 for 1 h. The cultures were then incubated with 10 μM of 2,7-dichlorofluorescein diacetate for 30 min at 37°C, washed with 0.01M, potassium phosphate buffer (PBS) (pH 7.4), centrifuged and subsequently lysed with saponin (0.15%) for 10 minutes at 4°C. Parasites were isolated by centrifugation at 1300 xg for 5 min at 10°C and lysed by sonication (30 s pulse, bath-type sonicator) at 4°C. Fluorescent intensities were recorded from the lysates in a spectrofluorometer (SpectraMax M3, Molecular Devices) at 502 nm and 523 nm excitation and emission wavelengths, respectively. Protein concentrations were determined in each well using the Pierce™ ModifiedLowry Protein Assay Kit (Thermo Scientific) and data was expressed as fluorescence intensity/milligram of parasite lysate protein.

DNA Isolation and Quantification

High molecular weight genomic DNA was isolated from WT, *pbggcs-ko* and *pbgr-ko* parasites using a Genomic DNA extraction Kit (Qiagen) following the manufacturer's instructions. Quantification of DNA was performed using the PicoGreen® dsDNA Quantitation Reagent (Molecular Probes®) with modifications as previously described [20, 21]. To determine the DNA concentration of the samples, a DNA standard curve was constructed using lambda DNA. The PicoGreen® excitation and emission fluorescence intensities were measured at 485 nm and 530 nm, respectively, using a fluorescence microplate reader (Wallac 1420 Victor^{2}™, PerkinElmer). The integrity of the genomic DNA was examined by analyzing the samples in a 0.8% ethidium bromide-containing agarose gel. The DNA was visualized using UV light (Gel Doc XR System, Bio-Rad).

Analysis of nuclear and mitochondrial DNA damage using the quantitative polymerase chain reaction (QPCR) assay

A QPCR assay was modified to determine the levels of DNA damage to the parasite's nuclear and mitochondrial genomes as we previously described [22]. The underlying

principle of the QPCR assay is that certain types of DNA lesions will prevent the DNA polymerase to effectively replicate the DNA fragment; thereby resulting in a decrease in the amplification yield. To ensure that the QPCR assay was performed within the linear range of amplification, optimal conditions for amplification of the nDNA and mtDNA fragments were determined by performing cycle and template tests. The initial DNA template concentration used for the amplification of nDNA and mtDNA was 5 ng and 7.5 ng, respectively. As a control to ensure quantitative conditions of amplification, a DNA sample with two fold the initial quantity of DNA concentration (10 ng and 15 ng of nDNA and mtDNA template, respectively) was amplified in duplicate. A 40–60% increase in amplification of the control target sequence was considered within the linear range of amplification and adequate for data analysis. To detect nDNA lesions a 6.1 kb fragment from the seryl-tRNA synthetase nuclear gene was amplified using the MasterAmp™ Extra-long PCR Reagents (Epicentre®). An initial denaturation was carried out for 45 s at 94°C, 24 cycles of denaturation for 15 s at 94°C, annealing-extension at 68°C for 12 min, and a final extension at 72°C for 10 min using the following primers: 5′-CACTATCAACATATTCATCTCTTGTTTC-3′ (forward) and 5′-GCTCTATGGACACCAATAGTTCCAAGGG-3′ (reverse).

To detect mtDNA lesions a fragment of 5.7 kb of the mitochondrial genome was amplified using 5′-GAATAGTGGTATAGTCATATCTCCATGAAC-3′ (forward) and 5′-TGGTATCTCGTAATGTAGAACAATAATAGG-3′ (reverse) as primers. The amplification conditions consisted on an initial denaturation for 45 s at 94°C, 21 cycles of denaturation for 15 s at 94°C and annealing-extension at 68°C for 12 min, and a final extension at 72°C for 10 min. To confirm that a single product of the expected size was obtained, the 6.1 kb and 5.7 kb PCR products were resolved on 1% ethidium bromide-stained agarose gels and visualized using UV-light (Gel Doc XR System, Bio-Rad). Nuclear and mitochondrial PCR products were quantified using PicoGreen. The background fluorescence was obtained from a sample without DNA template and subtracted from each experimental sample [20]. Background values were determined in duplicate. The results of *P. berghei* mutant parasites are expressed as DNA amplification levels relative to the levels of DNA amplification from WT parasites.

Quantification of mtDNA abundance by quantitative polymerase chain reaction (QPCR) assay

Because the number of mtDNA molecules vary between cells, it was critical to make certain that the amplification of the 5.7 kb mtDNA fragment was not affected by possible changes in the abundance of mtDNA molecules. A small mtDNA fragment of 186 bp was amplified to provide a precise measure of mtDNA molecules/abundance because small DNA fragments are unlikely to be damaged. Cycle and template tests were performed to establish optimal conditions of amplification. To assure quantitative PCR conditions, a DNA sample with 50% of the initial quantity of DNA concentration (2.5 ng) was amplified in duplicate. The PCR profile consisted on an initial denaturation for 45 s at 94°C, 25 cycles of denaturation for 15 s at 94°C, annealing for 45 s at 60°C and extension for 45 s at 72°C, and a final extension at 72°C for 10 min. The primer nucleotide sequences for the amplification of the 186 bp mtDNA fragment are 5′-ATTAACAACTATAGCATTATCTGGATGAGA-3′ (forward) and

5′-TTCTTTTTACATTTACATGGTAGCACTAAT-3′ (reverse). PCR products were quantified using PicoGreen after subtracting the background fluorescence. To confirm that a single product of 186 bp was amplified, PCR products were resolved on ethidium bromide-stained 2% polyacrylamide gels and visualized under UV-light (Gel Doc XR System, Bio-Rad). The abundance of mtDNA molecules of *P. berghei* mutant parasites is expressed relative to the mtDNA abundance in WT parasites.

Determination of DNA lesion frequencies

Because DNA lesions occur as independent events and, thus, are randomly distributed across the genome, the Poisson equation was used to calculate the frequency of DNA lesions per 10 kb/strand as previously described [22]. Using the Poisson distribution, $f\ x{=}e^{-\lambda}\frac{\lambda^x}{x!}$ a decrease in amplification is converted into lesion frequency considering that amplification is directly proportional to the portion of undamaged DNA templates (zero class molecules; x=0). Then, the average lesion frequency per DNA strand can be calculated as, $\lambda = -\ln A_D/A_O$ where A_D denotes the amount of amplification product of the damaged DNA template and A_O is the amplification product from undamaged DNA. The results of *P. berghei* mutant parasites are expressed as a relative amplification ratio (A_D/A_O) and as lesion frequency per 10 kb per strand relative to WT.

Quantification of protein carbonylations by the FTC fluorometric assay

Blood containing *P. berghei* parasites were harvested from infected mice with 5–15% parasitemia. White blood cells were removed using a Plasmodipur filter (Euro-Diagnostica), washed with 0.01 M PBS (pH 7.4), and the RBC pellet resuspended in 0.01 M PBS (pH 7.4), 1mM DTT, 0.5 mM PMSF and 1 mM EGTA followed by RBC lysis with 0.15% saponin. Samples were centrifuged at 1077 xg for 8 min and the parasite pellet was resuspended in protein isolation buffer (1% DOC and 10% SDS) containing a cocktail of protease inhibitors (0.01mg of leupeptin A, 0.001 mg of pepstatin A, 0.35 mg of PMSF). The supernatant was collected, and DTT was added to a final concentration of 75 mM, to avoid spontaneous protein oxidation, and stored at −80°C until further use. The protein concentration was determined using the Bicinchoninic acid (BCA) assay (Bio-Rad *DC*™ Protein Assay) or the *RC DC*™ Protein Assay (Bio-Rad). Infected blood was cultured for 24–28 h in complete RPMI medium in a low oxygen (10%) atmosphere as described above. Schizont cultures were harvested, diluted with 0.01 M PBS (pH 7.4), centrifuged, and subsequently lysed to obtain the parasite proteins as described above. Carbonyl content of proteins was assessed in parasites from mice blood (rings, trophozoites and schizonts) and in schizonts from cultures using a modified fluorometric assay [23]. Briefly, proteins (60 μg) were incubated with 50 μl of 0.2 mM fluorescein 5-thiosemicarbazide (FTC) overnight in the dark, precipitated with acetone, air dried, and solubilized with 50 μl of 6M guanidine hydrochloride. Protein precipitates were sonicated (30 s pulse, bath-type sonicator) for 10 min, vortexed, resuspended in 450 μl of 0.1 M PBS, vortexed, centrifuged (10,000 xg for 10 min at 4°C) and the supernatant aliquoted (150 μl/well) in triplicate into a black 96-well microplate (Thermo Scientific™). The fluorescence intensity was determined in a spectrofluorometer (Wallac 1420 VICTOR F) with excitation at 485 nm and emission at 535 nm. Protein concentrations were determined in each well using the Micro BCA™ Protein

Assay Kit (Pierce). The average of the fluorescence readings and the protein concentrations were measured in triplicate from 2–4 independent experiments. Nanomoles (nmol) of FTC-reacted carbonyls were calculated from the readings of FTC standard curve. Carbonyl content was expressed as nmol/milligram of parasite lysate protein.

Quantification of mRNA expression

Total RNA from parasite intraerythrocytic stages (5–15% parasitemia) was extracted using Tri-Reagent (Molecular Research Center, Inc.) following the manufacturer's instructions. Complementary DNA (cDNA) was synthesized using the SuperScript® VILO kit (Life Technologies). The *P. berghei* sequences of target genes were retrieved from PlasmoDB at plasmodb.org (Supplemental Table 1). Analysis of gene expression was done by RT-qPCR using the StepOnePlus™ System (Applied Biosystems) with the Fast SYBRR® Green Master Mix and 50 ng/μL of cDNA per sample. The samples were assayed in triplicate from three independent experiments. Gene expression data was analyzed using the StepOne™ Software v2.2 (Applied Biosystems) and normalized against the expression of 18S rRNA (Supplemental Table 1) [24] according to the $2^{-\Delta\,\Delta Ct}$ method [25, 26]. Melt curve analysis was used to confirm the specificity of amplified PCR products.

Modeling of Parasite Growth

A non-linear curve fit using the Weibull model for the growth curve of the parasite schizonts stages was applied $Y = Y_M - Y_M - Y_0\, e^{-(kx)^g}$. Parameters of this function were used to determine the delay in growth of the WT and mutant parasites. Specifically, Y_M corresponds to the maximum in the growth curve, Y_0 to the initial value of the growth curve, k to the time constant, g corresponds to a paremeter showing the inflection point of the growth, and t represents time. The g values from the fitted function were used to calculate the growth delay based on the parasitemia curves (Table 1).

Statistical Analysis

Statistical analyses were performed using GraphPad Prism v 5.0 (GraphPad Software Inc.). A p value <0.05 was considered statistically significant. Comparisons of the parasite stage percentages during parasitemia, and measurements of intraparasitic response to oxidative stress in the presence or absence of external H_2O_2, were made by Two-Way Analysis of Variance (Two-Way ANOVA) with Repeated Measures with post-hoc testing using a t-test with Bonferroni correction to account for multiple comparisons.

Diameter of parasites, DNA damage and protein carbonylation assays, were analyzed using One-Way ANOVA. A Two-Way ANOVA was used for the RT-qPCR data analysis. Both analyses were done using multiple comparisons with post-hoc testing using a t-test with Bonferroni corrections. A correlation matrix analysis was undertaken to find if there were associations between the biological variables measured and the parameters derived from the Weibull growth model used to analyze the parasitemia curves. The Pearson correlation coefficient was used as a measure of association. A p value of 0.05 was used to determine if a correlation in the matrix was significant (Table 2).

Results

Depleted GSH levels induce developmental delay and morphological changes during *P. berghei* intraerythrocytic growth

To assess the effects of GSH depletion on intraerythrocytic growth, the ring to schizont transition was monitored in synchronized cultures of the *pbggcs-ko1* and *pbggcs-ko*2 parasites and compared to WT parasites. Parasite clones from two independent transfections with a disrupted *ggcs* gene *(pbggcs*-ko1 and *pbggcs*-ko2) showed growth delay during the ring to schizont progression (Fig. 1). As depicted in Fig. 1, panels A, B, and C demonstrate an approximately two-hour delay during the ring to trophozoite transition, and an approximately 4 to 6-hour delay in the trophozoite to schizont transition. After 16 h, WT parasite cultures contained 12.4% rings, 85.9% trophozoites and 1.7% schizonts (Fig. 1A), while the mutant *pbggcs-ko1* and *pbggcs-ko2* parasites exhibit 33.3% and 41.1% rings ($p<0.05$; $p<0.001$) and 65.6% and 58.4% of trophozoites, respectively (Fig. 1B–C). Note that at 16 h, the *pbggcs-ko1* culture had only 1.1% of schizonts and no schizonts were detected in the *pbggcs-ko2* parasites (Fig. 1B–C). At 28 h, WT parasite cultures displayed 23.5% trophozoites and 76.5% schizonts, while the *pbggcs-ko1* and the *pbggcs-ko2* mutants presented 49.2% and 77.2% ($p<0.001$) trophozoites, and 50.8% ($p<0.05$) and 22.8% schizonts ($p<0.001$), respectively (Fig. 1B–C). The growth curves were analyzed separately for schizonts using a Weibull growth model. The results of the model fitting are shown in Table 1 and Fig. 1H. The non-linear fit of the schizont growth shows a decrease in the maximum level of growth of approximately 40% to 85% during the culture time period (Table 1), and also a change of time of the inflection point of the curve representing a two-hour growth delay (Fig. 1H).

The correlation matrix analysis showed that the inflection point (growth delay) correlated with the GSH levels present in each parasite clone (WT, 7.4 nmoles/10^9 parasites; *pbggcs-ko1,* 1.0 nmoles/10^9 parasites; *pbggcs-ko2,* 0.2 nmoles/10^9 parasites [14]) ($r^2=1.0$, $p = 0.013$). The complete correlation matrix is shown in Table 2. The upper triangular matrix shows the p values, while the lower triangular matrix (shaded in gray) shows the correlation coefficients. The only correlation that meets the statistical significance criterion is the association detected between the Weibull model parameter g and the levels of GSH. Due to sparsity of the data, more work is required to better understand this potentially causal correlation.

Morphological changes in the GSH deficient mutants, *pbggcs-ko1* and *pbggcs-ko2*, were assessed during the erythrocytic cycle (rings, trophozoites, schizonts) (Fig. 1D–G). Analysis of Diff-Quick stained cultured parasites revealed a significant size reduction and increased vacuolated cytoplasm in the mutants (Fig. 1G). A significant reduction in size was observed in both *pbggcs-ko1* and the *pbggcs*-ko*2* trophozoites at 16 h of culture ($p<0.05$ and $p<0.01$, respectively) and in schizonts at 24 and 28 h of culture ($p<0.001$ and $p<0.001$) (Fig. 1E–F). To further analyze the morphology, the number of parasites with vacuolated cytoplasm was determined. A remarkable number of the mutant parasites displayed vacuoles in their cytoplasm (60%, *pbggcs-ko1* and 45%, *pbggcs-ko2*), (Fig. 1G and Fig. S1–S3). These

results suggest that low GSH levels result in morphological changes and a significant delay of the intraerythrocytic development in *P. berghei.*

P. berghei ggcs deficient parasites display augmented intracellular oxidation of DCFH and an impaired response to oxidative stress

In order to determine whether depleted GSH is associated with an increase in oxidative stress, the green fluorescent intensity of DCF, the oxidation product of the nonfluorescent probe DCFH, was measured in WT and mutant parasites. The *pbggcs-ko2* (GSH levels: 0.2 nmoles/10^9 parasites [14]), show higher levels of DCF fluorescence under basal conditions when compared to WT parasites as depicted in Fig 2A (130–140 min; $p<0.05$, $p<0.01$). Similarly, DCF fluorescence under basal conditions is higher in *pbggcs-ko2* (1.9-fold) as compared to *pbgr-ko1* (GSH levels: 5.0 nmoles/10^9 parasites [15]) (Fig. 2A). There were no basal differences in intracellular oxidation, as determined by DCF fluorescence, between the *pbgr*-ko1 and the WT parasites.

To test the response to exogenous oxidative stress the parasites were exposed to H_2O_2. Treatment with 2 mM H_2O_2 had no effect on DCF fluorescent intensity in the WT or *pbgr-ko1* parasites (Fig. 2B). In contrast, incubation with H_2O_2 significantly increased (2.3 fold) the oxidation of DCFH in *pbggcs-ko2* parasites as compared to WT as depicted in Fig. 2B (100–140 min; $p<0.01$, $p<0.001$). Similarly, incubation of *pbggcs-ko2* with H_2O_2 significantly increased (2.5 fold) the oxidation of DCFH as compared to *pbgr-ko1* (110–140min; $p<0.05$, $p<0.01$, $p<0.001$) (Fig. 2B). These results suggest that the *pbggcs-ko2* parasites with low GSH levels exhibit higher basal oxidative stress and an impaired response to exogenous oxidative stress than the WT or the *pbgr-ko1* parasites.

pbggcs-ko parasites show increased levels of nuclear DNA damage

To investigate whether reduced GSH levels cause damage to the parasite's DNA, a QPCR assay was used to quantify the levels of nuclear (nDNA) and mitochondrial DNA (mtDNA) damage [22]. To measure nDNA damage in the WT, *pbggcs-ko* and *pbgr-ko* parasites, a 6.1 kb nDNA fragment of the *P. berghei* seryl t-RNA synthetase gene was amplified. The *pbggcs-ko2* parasites show a significant ($p<0.001$) 38.5% reduction in the amplification of the 6.1 kb nDNA fragment (Fig. 3A), indicating an increase in levels of nDNA damage (Fig. 3B), compared to WT, whereas the amplification levels of the 6.1 kb nDNA fragment from the *pbggcs-ko1*, *pbgr-ko1* and *pbgr-ko2* were similar to those of the WT parasites (Fig. 3A). The frequency of nDNA lesions was 10.6-fold higher for the *pbggcs-ko2* parasites compared to WT parasites ($p<0.01$) (Fig. 3B). However, no statistically significant differences in the number of nDNA lesions between the WT, the *pbggcs-ko1*, or *pbgr-ko* mutant parasites were detected.

The levels of mtDNA lesions in the WT and the mutant parasites were also determined by amplifying a 5.7 kb mtDNA fragment which represents 95% of the mitochondrial genome [27]. The analysis revealed no significant differences in the relative amplification of the mtDNA fragment between the *pbggcs-ko,* the *pbgr-ko* or the WT parasites, demonstrating no increase in mtDNA damage (Fig. 4A). Because high oxidative stress levels can affect the replication rates of the mtDNA, the steady-state levels of mtDNA molecules were assessed

in WT, *pbggcs-ko,* and *pbgr-ko*. Steady-state levels of mtDNA molecules were similar in the mutant and the WT parasites (Fig. 4B).

Collectively, these results suggest that parasites with reduced GSH levels show an increase in nDNA damage but no increase in damage to the mitochondrial genome.

Reduced GSH levels have no effect on protein carbonyl content in parasite intraerythrocytic stages

Protein carbonylation is one of the most common protein modifications caused by oxidative stress [28]. The extent of protein carbonylation was examined in total protein extracts from WT, *pbggcs-ko* and *pbgr-ko* mixed asynchronous blood stages and from synchronized schizonts cultures using the FTC fluorometric assay. The amount of carbonylated proteins from the intraerythrocytic blood stages of *pbggcs-ko* and *pbgr-ko* mutants was similar to those detected in the WT parasites (Fig. 5A). Similar results were obtained when protein carbonyls were measured using the dinitrophenylhydrazine (DNPH) method (Fig. S4). Cultured schizonts from mutant and WT parasites exhibited a 1.5–2.5 fold increase in carbonyl content as compared to the intraerythrocytic parasites (Fig. 5B; Table 3). However, no significant differences (One-way ANOVA and unpaired t-test) were observed between the mixed blood stages and cultured schizonts.

GSH depletion induces upregulation of genes involved in detoxification and DNA synthesis

To establish whether or not reduced GSH levels affects the expression of genes involved in oxidative detoxification and DNA synthesis, the mRNA levels of the superoxide dismutase (*sod)*, glutaredoxin (*grx)* and ribonucleotide reductase (*rnr)* genes were determined in the *pbggcs-ko2*, the *pbgr-ko1* and the WT parasites. Increased levels of *sod*, *grx* and *rnr* mRNA were detected in the *pbggcs-ko2* parasites as compared to the WT, while no differences in gene expression were observed between the *pbgr-ko1* and the WT parasites (Fig. 6). The *P. berghei* SOD, an enzyme responsible for the dismutation of the superoxide anion ($O_2^{\bullet -}$), was upregulated (9.6-fold induction) in the *pbggcs-ko2* parasites ($p<0.01$). The glutaredoxin (Grx) enzyme serves as a hydrogen-donor for RNR in the first step of DNA synthesis. Both *grx* and *rnr* genes showed a significant increase in expression in the *pbggcs-ko2* parasites, with 13.7 and 10-fold upregulation, respectively ($p<0.001$). These results suggest that *P. berghei* parasites exhibiting GSH depletion display increased expression of genes involved in ROS detoxification and DNA synthesis.

Discussion

Previous work from our laboratory showed that the *Plasmodium* GSH metabolism is dispensable for parasite development during the intraerythrocytic cycle [2, 3]. However, low GSH levels delayed progression of the infection in mice, presumably by extending the parasite's cellular cycle in order to compensate for the absence of the GSH antioxidant [2]. In this study we show that *pbggcs-ko* parasites with low GSH levels exhibit a delay in the ring to schizont progression, an impaired response to increased oxidative stress, and an increase in nDNA damage. In addition, we report an increased in mRNA expression of genes

involved in oxidative stress detoxification and DNA synthesis. These results suggest that optimal GSH levels are needed in order to protect the *P. berghei* nuclear genome from oxidative stress and for proper development. Furthermore, due to the impaired response to external oxidative stress, parasites will face a major hurdle to grow under conditions where environmental oxidative stress is high, such as the infected erythrocytes [3] and particularly the internal compartments of the mosquito host [14, 15].

In previous work, we reported that *pbggcs-ko* mutant parasites exhibit a delayed development in mice [14]. In this work we observed a two-hour delay in the transition from rings to trophozoites, and a 4 to 6-hour delay in the transition from trophozoites to schizonts when comparing the *pbggcs-ko1* and *pbgccs-ko2* mutants to the WT parasites. Our non-linear Weibull model of the schizont growth reveals a two-hour delay in the growth between the mutants and the WT parasites. Results from the present study also show a highly significant correlation between GSH levels and the delayed transition from ring to schizonts (r^2=1.0, p = 0.013), supporting the notion that GSH plays an important role on *Plasmodium* growth development. The observed delay and smaller size of the *pbggcs-ko* parasites suggest a slow-down in the cell cycle presumably to repair the oxidative damage observed in the nuclear genome. This is consistent with previous observations where a *Candida albicans* and a *Saccharomyces cerevisiae* strain harboring a deletion in the *ggcs* homologue, showed decreased growth rates and prolonged cell cycle [29, 30]. Additional evidence supporting the hypothesis that low GSH levels affect cell growth is provided by studies of human 3T3 fibroblasts treated with diethyl maleate, an agent that decreases nuclear GSH levels, resulted in slower cell cycle [31]. Similarly, we speculate that a longer cell cycle during *P. berghei* intraerythrocytic stages could provide the parasite with enough time to repair the oxidative damage to the nDNA occurring as a consequence of low GSH levels.

It should be pointed out that in contrast to *P. berghei*, deletion of the γGCS or glutathione synthetase genes was lethal for *P. falciparum*, suggesting that GSH levels are critical for *P. falciparum* development [32]. It is possible that *P. falciparum* is incapable of uptaking sufficient amounts of GSH from the mature RBC to allow parasite survival during the erythrocytic cycle [32, 33]. Furthermore, *P. falciparum* infected RBC display increased GSH efflux [34], which may result in a decrease in GSH available for parasite uptake. *P. berghei* prefers to invade young erythrocytes (reticulocytes), which are metabolically different from mature RBC, supporting the hypothesis that host environment have an impact in parasite growth and survival [34, 35]. Differences between both species should be taken into consideration and the GSH uptake in *P. berghei* be further evaluated, since the *pbggcs-ko* parasites have reduced but detectable GSH levels.

Plasmodium parasites depend on the digestion of hemoglobin as a major amino acid source. Heme/FP IX (Fe^{2+}/Fe^{3+}), generated as a by-product of Hb digestion, is toxic for the parasite and is detoxified via a biomineralization process into hemozoin, a chemically inert crystal that confers the distinctive pigment of *Plasmodium* parasites [36, 37, 38, 39]. However, some heme/FP IX (Fe^{2+}/Fe^{3+}) escapes the biomineralization process and reaches the cytosol [40,41] resulting in the generation of the superoxide ($O_2^{\bullet -}$) [4, 42]. The superoxide ($O_2^{\bullet -}$) can be dismutated by the cytosolic superoxide dismutase (SOD) to H_2O_2 and O_2 and can react with H_2O_2 to form the highly reactive hydroxyl radical (•OH) [3]. In addition, free iron

released from heme/FP IX (Fe^{2+}/Fe^{3+}) acts as a pro-oxidant mediating the generation of hydroxyl (•OH) via the Fenton reaction [3]. To maintain low levels of oxidants the parasites uses the GSH antioxidant system. The *pbggcs*-ko parasites, with low GSH levels are unable to detoxify the non-crystalized heme/FP IX and thus, will potentially have higher levels of free iron (Fe^{2+}/Fe^{3+}) and consequently higher levels of oxidative stress. It is plausible that in a low GSH environment like the one present in the *pbggcs-ko,* the parasites are unable to prevent the harmful effects of the FP IX; resulting in enhanced oxidative stress, leading to parasite growth delay and changes in the morphology during development. The H_2O_2 treatment significantly increased the oxidation of DCFH in the *pbggcs-ko2* parasites when compared to the WT and *pbgr-ko1* parasites, further supporting that low GSH levels are associated with increased oxidative stress. It is possible that the heme/FP IX (Fe^{2+}/Fe^{3+}) produced from Hb digestion may have promoted H_2O_2-induced DCFH oxidation. This idea is consistent with evidence showing that the H_2O_2-induced intracellular DCFH oxidation in bovine aortic endothelial cells is facilitated by uptake of iron mediated by the transferrin receptor [43]. Hence, we conclude that the mutant parasites have an impaired system to handle oxidative stress.

Our observations are consistent with studies where conditions leading to increased oxidative stress in *P. falciparum* cultures resulted in parasite growth delay [19, 44, 45]. Treatments that promote oxidative stress such as clotrimazole [19], pro-oxidant concentrations of curcumin [44] or bilirubin [45] result in increased accumulation of ROS and inhibition of parasite growth [19]. In addition, treatment with the antimalarial drug artesunate leads to increased oxidative stress and reduced GSH levels, causing parasite death [46]. The association between inhibition of parasite growth and increased oxidative stress was further supported by the addition of antioxidants that restored parasite growth [46]. Interestingly, our results show that the *pbgr-ko1* parasites with intermediate levels of GSH did not present growth delay (5.0 nmoles/10^9 parasites) [15] nor increased oxidation of DCFH. These data suggest that the increase in oxidative stress and the parasite growth delay are a consequence of reduced GSH levels as is the case for the *pbggcs-ko* parasites. We hypothesize that there is a threshold in the GSH levels required for normal *P. berghei* intraerythrocytic development.

Interestingly, an increase of nDNA damage was detected in *pbggcs-ko2* parasites with low GSH levels (0.2 nmoles/10^9 parasites [14]). This observation supports the notion that the increased oxidative stress associated with GSH depletion leads to the induction of oxidative damage in the *P. berghei* nuclear genome. Our findings are in agreement with a recent study in *P. falciparum* demonstrating that nDNA damage is associated with GSH depletion and increased oxidative stress after artesunate treatment [46]. It should be noted that neither the *pbgccs-ko1* (GSH levels of 1.0 nmoles/10^9 parasites [14]) nor the *pbgr-ko* mutants (GSH levels of 5.0 nmoles/10^9 parasites [15]) show a statistically significant increase in nDNA damage compared to WT (GSH levels of 7.4 nmoles/10^9 parasites [14]), demonstrating that only a drastic reduction in GSH levels (i.e. the 97% reduction in GSH levels detected in the *pbggcs-ko2* when compared to WT) are associated with increased oxidation of DCFH and nDNA damage. Surprisingly, increased mtDNA damage or changes in the abundance of mtDNA molecules in the *pbggcs-ko* parasites were not detected, suggesting that under physiological conditions, damage to the nDNA and not the mtDNA may lead to *P. berghei* growth delay. In contrast, *P. falciparum* parasites treated with high pro-oxidant

concentrations of curcumin resulted in increased damage to both the nuclear and mitochondrial genomes [44]. Mitochondria are the main ROS producers in the cell, mainly as a byproduct of oxidative phosphorylation [47]. Although *Plasmodium* parasites are fully capable of mitochondrial oxidative phosphorylation during the intraerythrocytic stages [48], they rely on anaerobic glycolysis as the main source of energy [49, 50] using the electron transport chain mainly for *de novo* pyrimidine biosynthesis [51, 52]. Our results showed that the absence of mtDNA damage under depleted GSH levels is in agreement with *Plasmodium* mitochondria not being the main source of ROS during the intraerythrocytic development. These results suggest that GSH plays a role in protecting the nuclear genome from oxidative stress.

Surprisingly, no significant changes in the amounts of protein carbonyl content in the *pbggcs-ko* or *pbgr-ko* parasites were detected in our analysis, suggesting that reduced GSH levels did not increase oxidative damage to proteins. Radfar *et al.* [53] reported that in *P. falciparum* cultures, chloroquine treatment led to an increase in protein carbonylation mainly in the mature schizont. Chloroquine is hypothesized to prevent hemozoin formation allowing the release of ferroprotoporphyrin IX (FP IX), which in turns induces oxidative stress (lethal to the parasite). Although a similar environment of increased oxidative stress is present in the *pbggcs-ko* mutants due to the significantly reduced GSH levels, our results show that the GSH deficiency did not further increase the levels of oxidized proteins neither in the intraerythrocytic stages nor in the synchronized schizont cultures.

The mRNA expression of *sod*, an enzyme responsible for the dismutation of O_2^- into H_2O_2 [54] was significantly upregulated in the *pbggcs-ko2* deficient parasites but not in *pbgr-ko2* parasites. The upregulation of cytosolic *sod* mRNA could be a protective response to the increased oxidative stress levels observed in the GSH depleted *pbggcs-ko2* mutants. The SOD enzyme represents an important antioxidant defense of *Plasmodium* parasites [55]. Two *Plasmodium* SODs have been identified, PfSOD1 and PfSOD2 [56], but the iron-dependent cytosolic PfSOD1 has been shown to be highly expressed in the intraerythrocytic stages [57]. Our results suggest that the extreme reduction of GSH levels in the *pbggcs-ko2* mutants induces an increase in the expression of the antioxidant genes presumably as a response to oxidative stress.

Optimal levels of dNTPs are required for DNA replication and DNA repair, a reaction catalyzed by RNR, the rate-limiting enzyme during DNA synthesis. The Grx enzyme can reduce RNR and exert redox regulation, cell growth and proliferation activities. Analysis of the *P. berghei* mutant parasites revealed that the *grx* and *rnr* genes displayed a significant increase in mRNA expression in the *pbggcs-ko2* parasites, while no differences were detected in the *pbgr-ko2* parasites. These results suggest that depletion of GSH is associated with a significant induction in the *grx* and *rnr* expression, probably in response to the oxidative damage observed in nDNA of the mutant parasites. These results are in agreement with findings showing induction of the RNR enzyme by DNA damage [58]. It is plausible that the *pbggcs-ko* parasites increased synthesis of dNTPs for DNA replication to compensate for deficiencies in proliferation or to repair the oxidative damage observed in the nDNA. However, these changes in gene expression are not detected in the *pbgr-ko2*

parasites, which show normal growth during the intraerythrocytic cycle [15] and no lesions in nDNA, suggesting that intermediate GSH levels are sufficient for normal parasite growth.

The reduced GSH levels present in the *pbggcs-ko* parasites have implications for antimalarial treatments [59]. We recently reported that the *pbggcs-ko* parasites were more sensitive to clearance after sub lethal doses of artemisinin (ART) treatment in a recrudescence assay [59]. These results suggest that GSH contributes to the ART response, making the parasites more tolerant to the drug. In addition, RRx-001, a new agent that inhibits the pentose phosphate pathway (PPP) of the parasite, was effective against *P. berghei* cerebral malaria and enhanced the activity of artemether when used in combination [60]. The PPP provides the only source of NADPH used by the parasite's GSH and the Trx systems during protection against the harmful effects of oxidative stress. This drug also binds to Hb and GSH, increasing the ROS levels and oxidative damage caused by artemether [61]. These reports together with our results encourage research to explore drugs that inhibit the GSH biosynthesis of the parasite as a potential combination drug for ART treatment.

This study provides evidence supporting that GSH deficient parasites exhibit a growth delay and damage to the nuclear genome during development of the intraerythrocytic stages. The reduced GSH levels did not increase damage to the parasite's mitochondrial genome nor protein carbonylation of the parasites. This report highlights a potential key role of GSH to support parasite development and to protect the nuclear genome from oxidative damage (Fig. 7). A threshold level of GSH appears to be necessary to observe the effects of oxidative stress in the parasite. Further work will be needed to clearly establish the existence of a GSH threshold level. Understanding the mechanisms that result in the inhibition of parasite development represents a promising approach for the development of new antimalarial drugs.

Supplementary Material

Refer to Web version on PubMed Central for supplementary material.

Acknowledgments

The authors want to thank Keila Crespo, Jesús F. Muñiz and Natalia Vega for technical support, Wieslaw Kozek for advice on microscopic analysis of parasite size and cytoplasmic vacuoles. This investigation was partially supported by the National Institute of General Medical Sciences, Research Centers in Minority Institutions Award G12RR03051, Minority Biomedical Research Support Grant 3S06-GM-008224 and Minority Biomedical Research-RISE Program Award R25-GM-061838. RGM was partially supported by National Institutes of Health Minority Access to Research Careers (MARC) grant: T36-GM-095335.

Abbreviations

ART	artemisinin
DCF	dichlorofluorescein
DCFH	2′, 7′-dichlorodihydrofluorescein
DHOD	dihydroorotate dehydrogenase

DNPH	dinitrophenylhydrazine
FP IX	ferritoprotoporphyrin IX
FTC	fluorescein 5-thiosemicarbazide
GR	glutathione reductase
Grx	Glutaredoxin
GSH	glutathione
GSSG	glutathione disulfide
H_2O_2	hydrogen peroxide
Hb	hemoglobin
mtDNA	mitochondrial DNA
nDNA	nuclear DNA
pbggcs-ko	*P. berghei* gamma-glutamylcysteine synthetase knockout
pbgr-ko	*P. berghei* glutathione reductase knockout
PBS	phosphate-buffered saline
PPP	Pentose phosphate pathway
QPCR	quantitative polymerase chain reaction
RBC	red blood cells
RNR	Ribonucleotide Reductase
ROS	reactive oxygen species
SOD	superoxide dismutase
Trx	thioredoxin
WT	wild type
γGCS	gamma glutamylcysteine synthetase

References

1. World Health Organization (WHO). [accessed 11.19.14] World Malaria Report 2014. 2014. http://www.who.int/malaria/publications/world_malaria_report_2014/en/index.html
2. Becker K, Tilley L, Vennerstrom JL, Roberts D, Rogerson S. Oxidative stress in malaria parasite-infected erythrocytes: host-parasite interactions. Int J Parasitol. 2004; 34:163–189. [PubMed: 15037104]
3. Müller S. Redox and antioxidant systems of the malaria parasite Plasmodium falciparum. Mol Microbiol. 2004; 53(5):1291–305. [PubMed: 15387810]

4. Tilley, L.; Loria, P.; Foley, M., editors. Antimalarial Chemotherapy. Vol. 2001. Humana Press; 2001. Chloroquine and other quinoline antimalarials; p. 87-121.
5. Krauth-Siegel RL, Bauer H, Schirmer RH. Dithiol proteins as guardians of the intracellular redox milieu in parasites: old and new drug targets in trypanosomes and malaria-causing plasmodia. Angew Chem Int Ed Engl. 2005; 44:690–715. [PubMed: 15657967]
6. Meister A. Selective modification of glutathione metabolism. Science. 1983; 220:472–477. [PubMed: 6836290]
7. Müller S, Gilberger TW, Krnajski Z, Lüersen K, Meierjohann S, Walter RD. Thioredoxin and glutathione system of malaria parasite Plasmodium falciparum. Protoplasma. 2001; 217:43–49. [PubMed: 11732337]
8. Atamna H, Ginsburg H. The malaria parasite supplies glutathione to its host cell: investigation of glutathione transport and metabolism in human erythrocytes infected with Plasmodium falciparum. Eur J Biochem. 1997; 250:670–679. [PubMed: 9461289]
9. Meister A, Anderson ME. Glutathione. Annual Reviews Biochemistry. 1983; 52:711–60.
10. Sies H. Glutathione and its role in cellular functions. Free Radic Biol Med. 1999; 27:916–921. [PubMed: 10569624]
11. Ginsburg H, Ward SA, Bray PG. An integrated model of chloroquine action. Parasitol Today. 1999; 15(9):357–60. [PubMed: 10461161]
12. Schirmer RH, Becker K, Matuschewski K. Depletion of *Plasmodium berghei* plasmoredoxin reveals a non-essential role for life cycle progression of the malaria parasite. PLoS One. 2008; 3(6):e2474. [PubMed: 18575607]
13. Buchholz K, Putrianti ED, Rahlfs S, Schirmer RH, Becker K, Matuschewski K. Molecular genetics evidence for the in vivo roles of the two major NADPH-dependent disulfide reductases in the malaria parasite. J Biol Chem. 2010; 285(48):37388–95. [PubMed: 20852334]
14. Vega-Rodríguez J, Dinglasan RR, Franke-Fayard B, Janse CJ, Pastrana-Mena R, Coppens I, Waters AP, Jacobs-Lorena M, Rodríguez-Orengo J, Serrano AE. The glutathione biosynthetic pathway is essential for mosquito transmission. PLoS Pathog. 2009; 5(2):e1000302. [PubMed: 19229315]
15. Pastrana-Mena R, Dinglasan RR, Franke-Fayard B, Vega-Rodriguez J, Fuentes-Caraballo M, Baerga-Ortiz A, Coppens I, Jacobs-Lorena M, Janse CJ, Serrano AE. Glutathione reductase-malaria parasites have normal blood stage growth but arrest during oocyst development in the mosquito. J Biol Chem. 2010; 285(35):27045–56. [PubMed: 20573956]
16. Janse CJ, Franke-Fayard B, Mair GR, Ramesar J, Thiel C, Engelmann S, Matuschewski K, van Gemert GJ, Sauerwein RW, Waters AP. High efficiency transfection of Plasmodium berghei facilitates novel selection procedures. Mol Biochem Parasitol. 2006; 145(1):60–70. [PubMed: 16242190]
17. Janse CJ, Water AP. Plasmodium berghei: the application of cultivation and purification techniques to molecular studies of malaria parasites. Parasitol Today. 1995; 11:138–43. [PubMed: 15275357]
18. Waters AP, Thomas AW, van Dijk MR, Janse CJ. Transfection of malaria parasites. Methods. 1997; 13(2):134–47. [PubMed: 9405197]
19. Trivedi V, Chand P, Srivastava K, Puri SK, Maulik PR, Bandyopadhyay U. Clotrimazole inhibits hemoperoxidase of Plasmodium falciparum and induces oxidative stress. Proposed antimalarial mechanism of clotrimazole. J Biol Chem. 2005; 280(50):41129–36. [PubMed: 15863504]
20. Acevedo-Torres K, Berríos L, Rosario N, Dufault V, Skatchkov S, Eaton MJ, Torres-Ramos CA, Ayala-Torres S. Mitochondrial DNA damage is a hallmark of chemically induced and the R6/2 transgenic model of Huntington's disease. DNA Repair. 2009; 8(1):126–36. [PubMed: 18935984]
21. Siddiqui A, Rivera-Sánchez S, del Castro MR, Acevedo-Torres K, Rane A, Torres-Ramos CA, Nicholls DG, Andersen JK, Ayala-Torres S. Mitochondrial DNA damage is associated with reduced mitochondrial bioenergetics in Huntington's disease. Free Radic Biol Med. 2012; 53(7): 1478–88. [PubMed: 22709585]
22. Ayala-Torres S, Chen Y, Svoboda T, Rosenblatt J, Van Houten B. Analysis of gene-specific DNA damage and repair using quantitative polymerase chain reaction. Methods. 2000; 22:135–147. [PubMed: 11020328]
23. Mohanty JG, Bhamidipaty S, Evans MK, Rifkind JM. A fluorimetric semi-microplate format assay of protein carbonyls in blood plasma. Anal Biochem. 2010; 400(2):289–94. [PubMed: 20122892]

24. Yano K, Komaki-Yasuda K, Kobayashi T, Takemae H, Kita K, Kano S, Kawazu S. Expression of mRNAs and proteins for peroxiredoxins in Plasmodium falciparum erythrocytic stage. Parasitol Int. 2005; 54(1):35–41. [PubMed: 15710548]
25. Schmittgen TD, Livak KJ. Analyzing real-time PCR data by the comparative Ct method. Nature Protocols. 2008; 3(6):1101–1108. [PubMed: 18546601]
26. Yuan JS, Reed A, Chen F, Stewart CN Jr. Statistical analysis of real-time PCR data. BMC Bioinformatics. 2006; 7:85. [PubMed: 16504059]
27. Vaidya AB, Akella R, Suplick K. Sequences similar to genes for two mitochondrial proteins and portions of ribosomal RNA in tandemly arrayed 6-kilobase-pair DNA of a malarial parasite. Mol Biochem Parasitol. 1989; 35(2):97–107. [PubMed: 2549417]
28. Stadtman ER, Levine RL. Free radical-mediated oxidation of free amino acids and amino acid residues in proteins. Amino Acids. 2003; 25:207–18. [PubMed: 14661084]
29. Yadav AK, Desai PR, Rai MN, Kaur R, Ganesan K, Bachhawat AK. Glutathione biosynthesis in the yeast pathogens Candida glabrata and Candida albicans: essential in C. glabrata, and essential for virulence in C. albicans. Microbiology. 2011; 157(2):484–95. [PubMed: 20966090]
30. Sharma KG, Sharma V, Bourbouloux A, Delrot S, Bachhawat AK. Glutathione depletion leads to delayed growth stasis in Saccharomyces cerevisiae: evidence of a partially overlapping role for thioredoxin. Curr Genet. 2000; 38:71–77. [PubMed: 10975255]
31. Markovic J, Mora NJ, Broseta AM, Gimeno A, de-la-Concepción N, Viña J, Pallardó FV. The depletion of nuclear glutathione impairs cell proliferation in 3t3 fibroblasts. PLoS One. 2009; 4(7):e6413. [PubMed: 19641610]
32. Patzewitz EM, Wong EH, Müller S. Dissecting the role of glutathione biosynthesis in Plasmodium falciparum. Mol Microbiol. 2012; 83(2):304–18. [PubMed: 22151036]
33. Müller S. Role and regulation of glutathione metabolism in Plasmodium falciparum. Molecules. 2015; 20(6):10511–34. [PubMed: 26060916]
34. Barrand MA, Winterberg M, Ng F, Nguyen M, Kirk K, Hladky SB. Glutathione export from human erythrocytes and Plasmodium falciparum malaria parasites. Biochem J. 2012; 448(3):389–400. [PubMed: 22950671]
35. Srivastava A, Creek DJ, Evans KJ, De Souza D, Schofield L, Müller S, Barrett MP, McConville MJ, Waters AP. Host reticulocytes provide metabolic reservoirs that can be exploited by malaria parasites. PLoS Pathog. 2015; 11(6):e1004882. [PubMed: 26042734]
36. Fitch CD, Kanjananggulpan P. The state of ferriprotoporphyrin IX in malaria pigment. J Biol Chem. 1987; 262(32):15552–5. [PubMed: 3119578]
37. Pagola S, Stephens PW, Bohle DS, Kosar AD, Madsen SK. The structure of malaria pigment beta-haematin. Nature. 2000; 404(6775):307–10. [PubMed: 10749217]
38. Egan TJ, Combrinck JM, Egan J, Hearne GR, Marques HM, Ntenteni S, Sewell BT, Smith PJ, Taylor D, van Schalkwyk DA, Walden JC. Fate of haem iron in the malaria parasite Plasmodium falciparum. Biochem J. 2002; 365:343–347. [PubMed: 12033986]
39. Hempelmann E. Hemozoin biocrystallization in Plasmodium falciparum and the antimalarial activity of crystallization inhibitors. Parasitol Res. 2007; 100(4):671–6. [PubMed: 17111179]
40. de Almeida Ribeiro MC, Augusto O, da Costa Ferreira AM. Influence of quinoline-containing antimalarials in the catalase activity of ferriprotoporphyrin IX. J Inorg Biochem. 1997; 65:15–23.
41. Loria P, Miller S, Foley M, Tilley L. Inhibition of the peroxidative degradation of haem as the basis of action of chloroquine and other quinoline antimalarials. Biochem J. 1999; 339:363–370. [PubMed: 10191268]
42. Liochev SI, Fridovich I. Superoxide and iron: partners in crime. IUBMB Life. 1999; 48(2):157–61. [PubMed: 10794591]
43. Tampo Y, Kotamraju S, Chitambar CR, Kalivendi SV, Keszler A, Joseph J, Kalyanaraman B. Oxidative stress-induced iron signaling is responsible for peroxide-dependent oxidation of dichlorodihydrofluorescein in endothelial cells: role of transferrin receptor-dependent iron uptake in apoptosis. Circ Res. 2003; 92(1):56–63. [PubMed: 12522121]
44. Cui L, Miao J, Cui L. Cytotoxic effect of curcumin on malaria parasite Plasmodium falciparum: inhibition of histone acetylation and generation of reactive oxygen species. Antimicrob Agents Chemother. 2007; 51(2):488–94. [PubMed: 17145789]

45. Kumar S, Guha M, Choubey V, Maity P, Srivastava K, Puri SK, Bandyopadhyay U. Bilirubin inhibits Plasmodium falciparum growth through the generation of reactive oxygen species. Free Radic Biol Med. 2008; 44(4):602–13. [PubMed: 18070610]
46. Gopalakrishnan AM, Kumar N. Antimalarial action of artesunate involves DNA damage mediated by reactive oxygen species. Antimicrob Agents Chemother. 2015; 59(1):317–25. [PubMed: 25348537]
47. Saraste M. Oxidative phosphorylation at the fin de siècle. Science. 1999; 283(5407):1488–93. [PubMed: 10066163]
48. Kawahara K, Mogi T, Tanaka TQ, Hata M, Miyoshi H, Kita K. Mitochondrial dehydrogenases in the aerobic respiratory chain of the rodent malaria parasite Plasmodium yoelii yoelii. J Biochem. 2009; 145(2):229–37. [PubMed: 19060309]
49. Bryant C, Voller A, Smith MJ. The incorporation of radioactivity from (14C) glucose into the soluble metabolic intermediates of malaria parasites. Am J Trop Med Hyg. 1964; 13:515–19. [PubMed: 14196045]
50. Scheibel LW, Pflaum WK. Cytochrome oxidase activity in platelet-free preparations of Plasmodium falciparum. J Parasitol. 1970; 56(6):1054. [PubMed: 4323401]
51. Gutteridge WE, Dave D, Richards WH. Conversion to dihydroorotate to orotate in parasitic protozoa. Biochem Biophys Acta. 1979; 582(3):390–401. [PubMed: 217438]
52. Painter HJ, Morrisey JM, Mather MW, Vaidya AB. Specific role of mitochondrial electron transport in blood-stage Plasmodium falciparum. Nature. 2007; 446(7131):88–91. [PubMed: 17330044]
53. Radfar A, Diez A, Bautista JM. Chloroquine mediates specific proteome oxidative damage across the erythrocytic cycle of resistant Plasmodium falciparum. Free Radic Biol Med. 2008; 44:2034–42. [PubMed: 18397762]
54. McCord JM, Fridovich I. Superoxide dismutase. An enzymic function for erythrocuprein (hemocuprein). J Biol Chem. 1969; 244(22):6049–55. [PubMed: 5389100]
55. Bécuwe P, Gratepanche S, Fourmaux MN, Van Beeumen J, Samyn B, Mercereau-Puijalon O, Touzel JP, Slomianny C, Camus D, Dive D. Characterization of iron-dependent endogenous superoxide dismutase of Plasmodium falciparum. Mol Biochem Parasitol. 1996; 76(1–2):125–34. [PubMed: 8920001]
56. Sienkiewicz N, Daher W, Dive D, Wrenger C, Viscogliosi E, Wintjens R, Jouin H, Capron M, Müller S, Khalife J. Identification of a mitochondrial superoxide dismutase with an unusual targeting sequence in Plasmodium falciparum. Mol Biochem Parasitol. 2004; 137(1):121–32. [PubMed: 15279958]
57. Bozdech Z, Ginsburg H. Antioxidant defense in Plasmodium falciparum--data mining of the transcriptome. Malar J. 2004; 3:23. [PubMed: 15245577]
58. Elledge SJ, Davis RW. DNA damage induction of ribonucleotide reductase. Mol Cell Biol. 1989; 9(11):4932–4940. [PubMed: 2513480]
59. Vega-Rodríguez J, Pastrana-Mena R, Crespo-Lladó KN, Ortiz JG, Ferrer-Rodríguez I, Serrano AE. Implications of glutathione levels in the Plasmodium berghei response to chloroquine and artemisinin. PLoS One. 2015; 10(5):e0128212. [PubMed: 26010448]
60. Yalcin O, Oronsky B, Carvalho LJ, Kuypers FA, Scicinski J, Cabrales P. From METS to malaria: RRx-001, a multi-faceted anticancer agent with activity in cerebral malaria. Malar J. 2015; 14:218. [PubMed: 26017006]
61. Scicinski J, Oronsky B, Taylor M, Luo G, Musick T, Marini J, Adams CM, Fitch WL, Elledge SJ, Davis RW. DNA damage induction of ribonucleotide reductase. Mol Cell Biol. 1989; 9(11):4932–4940. [PubMed: 2513480]
62. del Castro MR, Suarez E, Kraiselburd E, Isidro A, Paz J, Ferder L, Ayala-Torres S. Aging increases mitochondrial DNA damage and oxidative stress in liver of rhesus monkeys. Exp Gerontol. 2012; 47(1):29–37. [PubMed: 22027539]

Highlights

- Decreased GSH levels correlate with a delay of the ring to schizont transition.
- Damage to the nDNA but not the mtDNA is higher in GSH-deficient parasites.
- Optimal GSH levels are required for parasite normal growth and to avoid nDNA damage

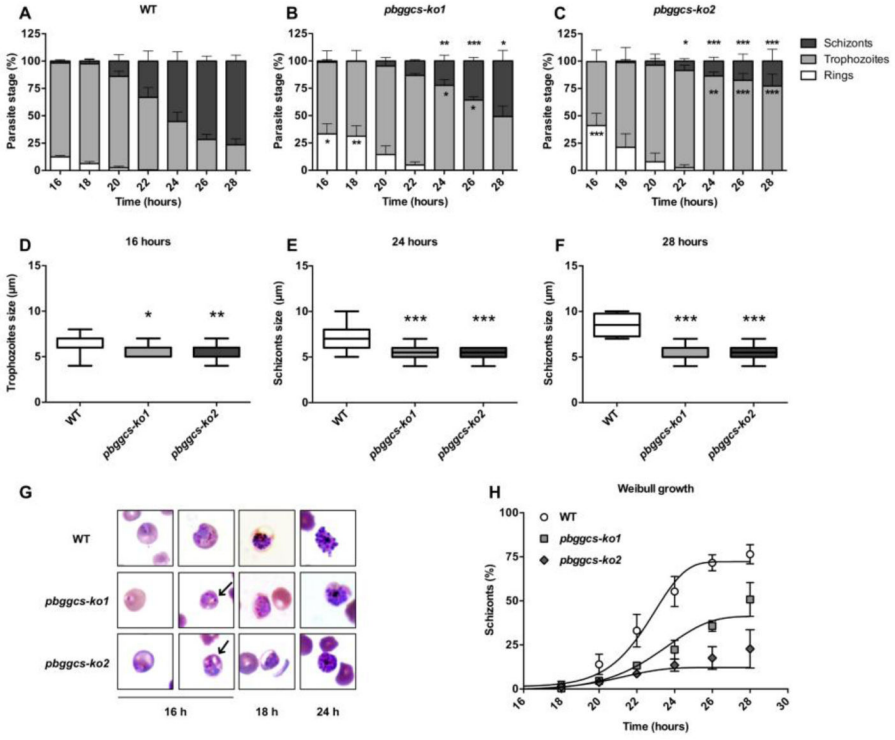

Figure 1. *In vitro* development of WT and *pbggcs-ko* parasites

(A–C) Percentage of intraerythrocytic stages of WT (A), *pbggcs-ko1* (B), and *pbggcs-ko2* (C) parasites throughout a 28 h time course. Three morphological stages were distinguished by microscopy: rings (white bars), trophozoites (light grey bars), and schizonts (dark grey bars). (D–F) The size of trophozoites and schizonts stages from WT (white box), *pbggcs-ko1* (light grey box) and *pbggcs-ko2* (dark grey box) parasites are shown at 16 (D), 24 (E) and 28 h (F) (n=20). (G) Representative images of intraerythrocytic stages of WT, *pbggcs-ko1* and *pbggcs-ko2* parasites at 16, 24 and 28 h of *in vitro* culture. Cytoplasmic vacuoles are indicated by arrows. (H) Weibull growth model for the percentage of schizonts for WT (circle), *pbggcs*-ko1 (square) and *pbggcs*-ko2 (diamond) parasites. Significant differences were observed between the WT parasites and the *pbggcs-ko1* and *pbggcs*-ko2 mutant parasites (*p<0.05, **p<0.01, ***p<0.001) analyzed by Two-way repeated measures ANOVA with Bonferroni multiple comparison test. Bars represent the SEM from 3 independent experiments.

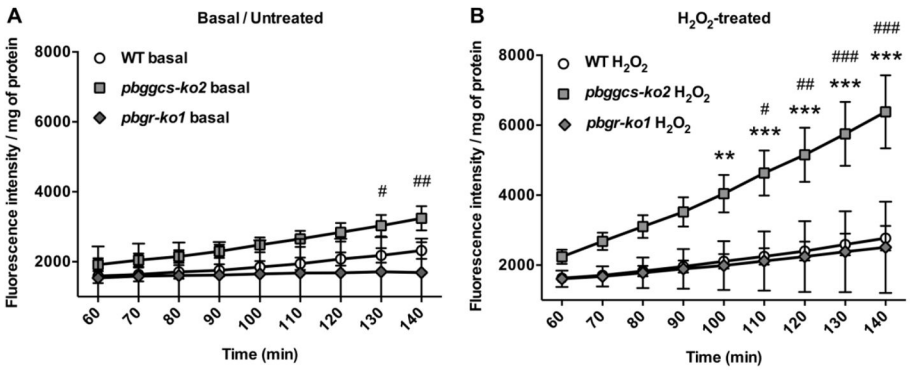

Figure 2. *P. berghei ggcs-ko* parasites show increased levels of intracellular oxidative stress

DCF fluorescence intensity was determined at various time points in basal/untreated and H_2O_2-treated *in vitro* cultures of WT, *pbggcs-ko2* and *pbgr-ko1* parasites. Cultures were treated with 2 mM H_2O_2 for 1 h. (A) Basal levels of DCF fluorescence in WT, *pbggcs-ko2* and *pbgr-ko1* parasites. (B) H_2O_2-induced DCF fluorescence intensity in WT, *pbggcs-ko2* and *pbgr-ko1* parasites. Significant differences were observed between the H_2O_2-treated WT and *pbggcs-ko2* (**p<0.01, ***p<0.001) and *pbggcs-ko2* and *pbgr-ko1* mutant parasites (#p<0.05, ##p<0.01, ###p<0.001) at different time points analyzed by Two-way repeated measures ANOVA with Bonferroni multiple comparison test. Bars represent the SD from 2 (*pbgr-ko1*) and SEM from 4 (*pbggcs-ko2*) independent experiments.

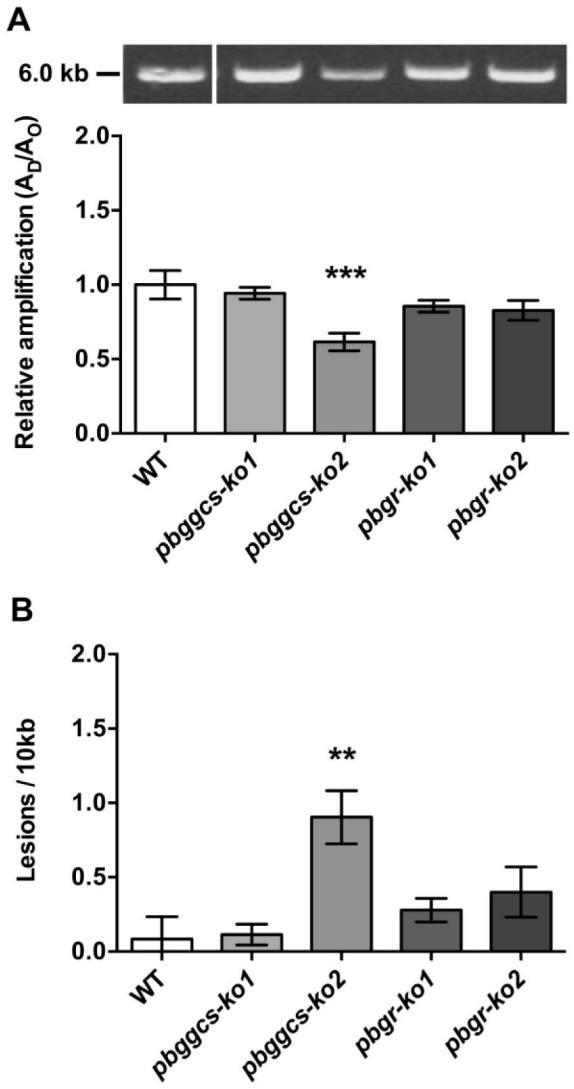

Figure 3. *P. berghei ggcs-ko2* mutant shows increased levels of nDNA damage

(A) Upper panel, representative gel showing the amplification of a 6.1 kb nDNA fragment of the seryl t-RNA synthetase gene from WT, *pbggcs-ko* and *pbgr-ko* parasites. Lower panel, relative amplification levels of the 6.1 kb nDNA fragment from WT and mutant parasites. (B) Frequency of nDNA lesions per 10 kb per strand was calculated as described in Materials and Methods. Representative results of the 6.1 kb amplified fragment are shown in the upper panel. The 6 kb molecular weight marker is indicated in the left. Significant differences were observed between WT and *pbggcs-ko2* parasites (**p<0.01, ***p<0.001) analyzed by One-way ANOVA with Bonferroni multiple comparison test. Bars represent the SEM from 3 independent experiments and 10 QPCR analyses.

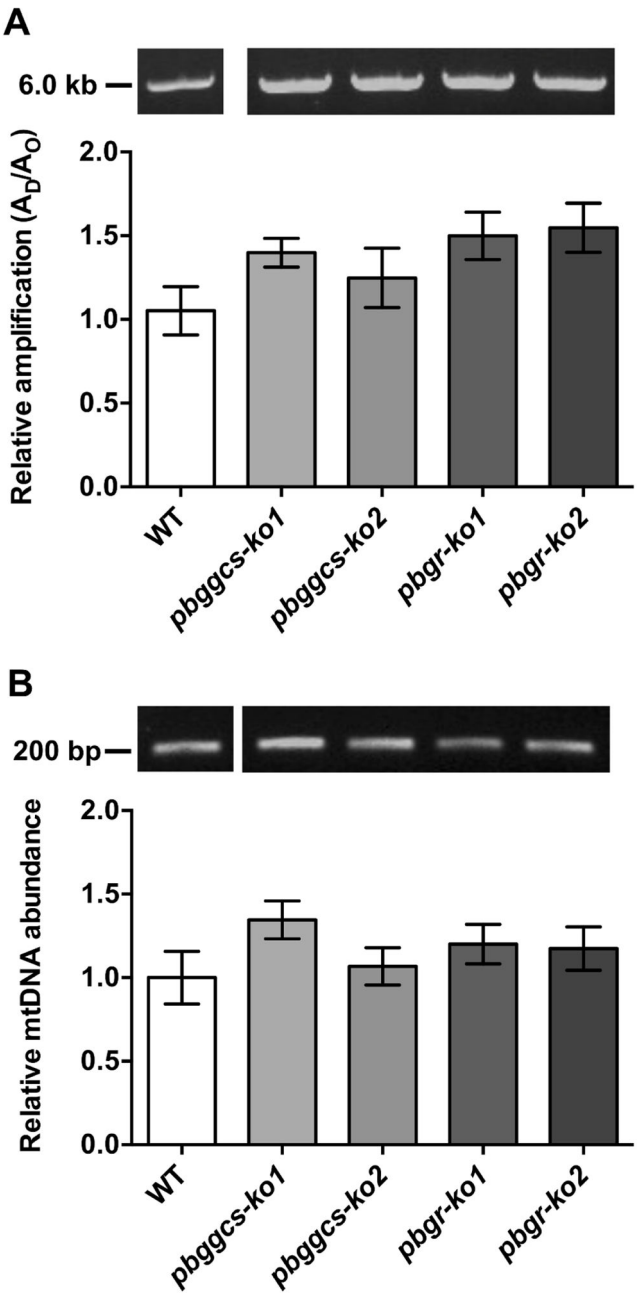

Figure 4. Mutant parasites show no changes in the levels of mtDNA damage or mtDNA abundance

(A) Upper panel, representative gel showing the amplification of a 5.7 kb mtDNA fragment from WT, *pbggcs-ko* and *pbgr-ko* parasites. Lower panel, relative amplification of a 5.7 kb mtDNA fragment that was normalized for changes in mtDNA abundance. (B) Upper panel, representative gel showing the amplification of the 186 bp mtDNA fragment. Lower panel, relative amplification of a 186 bp mtDNA fragment representative of mitochondrial abundance. No significant differences in mtDNA damage or mtDNA abundance were observed between WT and mutant parasites. Bars represent the SEM from 3 independent

experiments, and 14 and 12 QPCR analyses for mtDNA damage or mtDNA abundance, respectively.

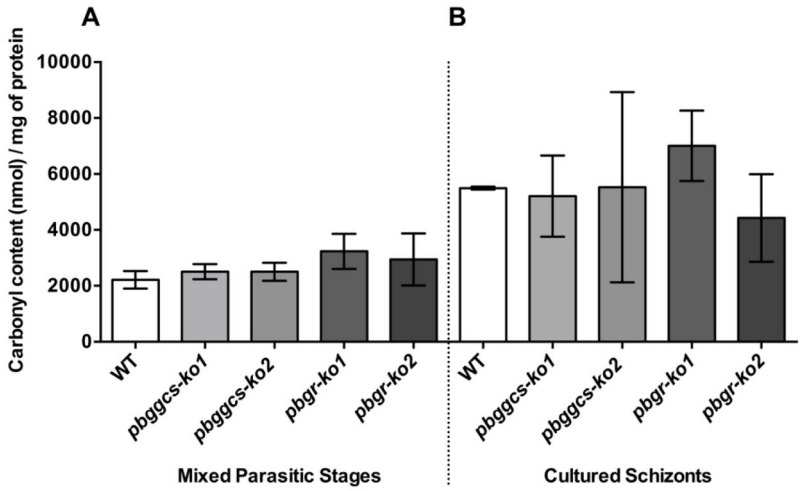

Figure 5. Levels of protein carbonylation in intraerythrocytic stages from WT and mutant parasites

Levels of protein carbonylation were assessed in WT, *pbggcs-ko*, and *pbgr-ko* parasites using the FTC fluorescent assay. Panel A: protein carbonyl content in intraerythrocytic asynchronous blood stages. Panel B: protein carbonyl content in cultured schizonts. No significant differences in the levels of protein carbonylations were observed between WT and mutant intraerythrocytic asynchronous parasites and cultured schizonts. Bars represent the SEM of 4 independent experiments from intraerythrocytic stages and SD of 2 independent experiments from cultured schizonts.

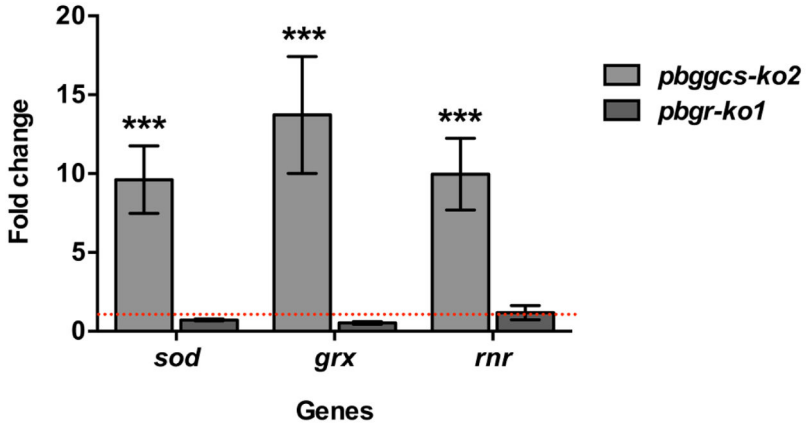

Figure 6. ***P. berghei ggcs-ko*** **parasites show upregulated levels of** ***sod, grx*** **and** ***rnr*** **mRNA expression**

The relative gene expression was determined by RT-qPCR and expressed as fold change for the *pbggcs-ko2* and *pbgr-ko2* as compared to WT. The data was normalized against the expression of 18S rRNA. The *sod* (superoxide dismutase), *grx* (glutaredoxin) and *rnr* (ribonucleotide reductase) genes showed increased gene expression in the *pbggcs-ko2* mutant parasites (***$p<0.001$) analyzed by Two-way ANOVA with Bonferroni multiple comparison test. Bars represent the SEM from 3 independent experiments. Red dotted line represents the expression level in WT parasites.

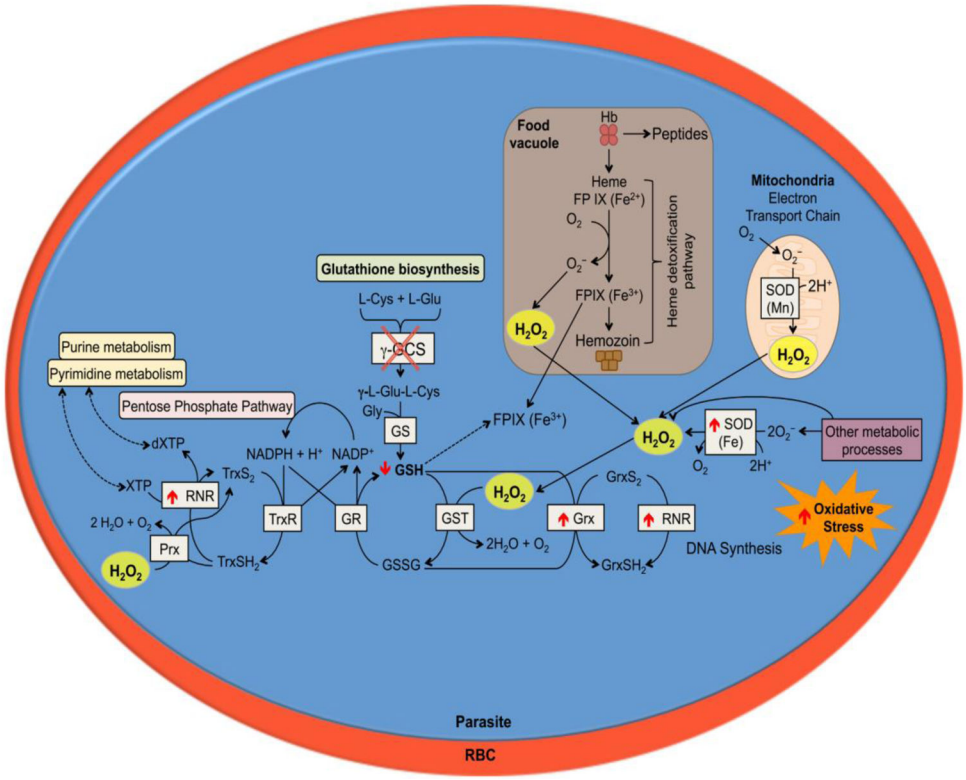

Figure 7. Proposed effects of GSH deficiency in *P. berghei* during asexual blood stages

Representation of the *P. berghei* intracellular blood stage with the biochemical processes involved in the antioxidant defense. The red circle represents the red blood cell and the blue circle represents the parasite and the biochemical antioxidant pathways. The *pbggcs-ko* mutant parasites with significantly low GSH levels exhibit growth delay during intraerythrocytic development probably due to an impaired response to oxidative stress and nDNA damage. As a result of increased oxidative stress, the *pbggcs-ko* mutant parasites increase expression of *sod* for cytosolic dismutation of the superoxide, and *grx* and *rnr* to support dNTP synthesis. These events may be necessary to sustain development of *P. berghei* parasite in the absence of GSH.

Table 1

Non-linear fit Weibull Growth Model

Best-fit values	**WT**	***pbggcs-ko1***	***pbggcs-ko2***
Y_M	72.22	41.24	12.20
Y_0	1.366	−0.4789	−0.3949
k	0.04333	0.04197	0.04640
g	15.14	11.65	11.15

Table 2

Correlation Matrix Analysis and p Values

	Parameter g	Parameter k	DNA damage	GSH levels
Parameter g		0.786	0.504	0.013
Parameter k	−0.330		0.282	0.798
DNA damage	0.703	−0.904		0.517
GSH levels	1.000	−0.311	0.688	

Table 3

Protein Carbonylation Content in Wild Type versus Mutant Parasites

	WT	***pbggcs*-ko1**	***pbggcs*-ko2**	***pbgr*-ko1**	***pbgr*-ko2**
Mixed Asexual Stages (nmol/mg ± SEM)	2216 ± 312	2506 ± 272	2502 ± 320	3234 ± 630	2945 ± 931
Schizonts Stages (nmol/mg ± SD)	5496 ± 55	5207 ± 1452	5526 ± 3401	7006 ± 1257	4428 ± 1568
Fold	**2.48**	**2.08**	**2.21**	**2.17**	**1.50**